American Mineralogist, Volume 97, pages 1394–1401, 2012

Structural relaxation in tetrahedrally coordinated Co^{2+} along the gahnite-Co-aluminate spinel solid solution

Matteo Ardit,[1,*] Giuseppe Cruciani,[1] and Michele Dondi[2]

[1]Earth Science Department, University of Ferrara, via Saragat 1, 44100 Ferrara, Italy
[2]Institute of Science and Technology for Ceramics (ISTEC-CNR), via Granarolo 64, 48018 Faenza, Italy

Abstract

The structural relaxation around the Co^{2+} ion along the gahnite ($ZnAl_2O_4$)-Co-aluminate ($CoAl_2O_4$) join was investigated by a combined X-ray diffraction (XRD) and electronic absorption spectroscopy (EAS) approach. Monophasic spinel samples ($Zn_{1-y}Co_yAl_2O_4$ with y = 0, 0.25, 0.5, 0.75, and 1 apfu) were obtained through solid-state reaction (1300 °C with slow cooling). The cobalt incorporation induces a linear increase of the unit-cell parameter (a) accompanied by an increasing inversion parameter (up to 0.07) so that the Co^{2+} for Al^{3+} substitution in the octahedral site is, at a first approximation, the cause of the lattice expansion. However, a careful consideration of T-O distances highlights the role played by an enhanced covalence degree of Zn-O bonds. The optical spectra are characterized by the occurrence of electronic transitions of Co^{2+} in tetrahedral coordination affected by a strong spin-orbit coupling, causing a threefold splitting of spin-allowed bands. Further complications stem from mixing of quadruplet and doublet states (leading to a consistent intensity gain of spin-forbidden bands) and vibronic effects (producing intense sidebands). Crystal field strength goes from 4187 to 4131 cm^{-1} with increasing cobalt amount, while the Racah B parameter is in the 744–751 cm^{-1} range (C ~3375 cm^{-1}). To achieve a reliable estimation of the local Co-O distance, the tetrahedral distance evolution was recast to eliminate the effects of the inversion degree. By this way, a relaxation coefficient as low as $\varepsilon = 0.47$ was obtained, i.e., significantly smaller than literature data for other spinel systems. The gahnite-Co-aluminate join seems to be constrained by the strong preference of Zn^{2+} for the tetrahedral site in which its enhanced covalency can be exerted, limiting the cation exchange between tetrahedral and octahedral sites as well as the lattice flexibility.

Keywords: Gahnite, Co-aluminate, spinel structure, X-ray powder diffraction, Rietveld refinement, electronic absorption spectroscopy, structural relaxation

Introduction

In the last decades, several studies have demonstrated that the stability of isostructural solid solutions, at the atomic scale, is affected by a structural relaxation around substituting cations (e.g., Galoisy 1996; Langer 2001; Langer et al. 2004; Taran et al. 2004; Andrut et al. 2004). Along a binary join, the average structure obtained by diffraction methods does not give any indication on the local mean distances between the central ion and its surrounding oxygen-based polyhedron. The lack of this information may be overcome by the use of spectroscopic methods. As proposed by Urusov (1992), the deviation from the Vegard's rule can be quantified, on a geometrical basis, through the relaxation coefficient (ε), as:

$$\varepsilon = (\langle B\text{-O}\rangle_{y\to 0} - \langle A\text{-O}\rangle)\cdot(\langle B\text{-O}\rangle - \langle A\text{-O}\rangle)^{-1} \quad (1)$$

where, for a hypothetic $A_{1-y}B_yO$ solid solution, $\langle A\text{-O}\rangle$ and $\langle B\text{-O}\rangle$ are the mean polyhedral distances for the two end-members (measured for instance by XRD), and $\langle B\text{-O}\rangle_{y\to 0}$ is the local mean distance for $A_{1-y}B_yO$, with $y\to 0$ (estimated by spectroscopy). The behavior of exchanging cations in a solid solution falls between two extreme cases deriving from the Equation 1. The case of full relaxation, i.e., the situation implied by the hard sphere (*HS*) model, $\varepsilon = 1$, means that the interatomic $\langle B\text{-O}\rangle_{y\to 0}$ distance will not change with composition: $\langle B\text{-O}\rangle_{y\to 0} = \langle B\text{-O}\rangle$. In absence of relaxation, on the other side, $\varepsilon = 0$ (corresponding to the Vegard's additivity rule predicted by the virtual crystal approximation, *VCA*, model), therefore $\langle B\text{-O}\rangle_{y\to 0} = \langle A\text{-O}\rangle$ (Wildner et al. 2004; Andrut et al. 2004). It follows that the accurate determination of the local structure around substituting ions is fundamental to provide detailed information on their incorporation and on physical properties: for instance, the presence of transition metal ions as impurities is one of the most important and studied causes of color in minerals and synthetic analogs (e.g. Gaudry et al. 2006; Juhin et al. 2007, 2008; Cruciani et al. 2009; Hålenius et al. 2010). Although evidences of a large deviation from the Vegard's rule in tetrahedral site were already reported for simple binary solid solutions (e.g., Levelut et al. 1991), the above mentioned structural relaxation studies about silicate and oxide solid solutions of geological interest are mainly focused on cation substitution in octahedral coordination sites. The only exception is represented by the work of Hålenius et al. (2011) where the effects of the tetrahedral Mn^{2+}-Mg substitution were assessed along the $MgAl_2O_4$-$MnAl_2O_4$ spinel join.

Minerals belonging to the spinels group are ternary oxides

* E-mail: rdtmtt@unife.it

0003-004X/12/0809-1394$05.00/DOI: http://dx.doi.org/10.2138/am.2012.4093

with general formula AB_2O_4 that crystallize in the cubic crystal system (space group $Fd\bar{3}m$; $Z = 8$) with the oxygen anions arranged in a cubic close-packed lattice. The unit cell contains 32 oxygen atoms (with the atomic coordinate conventionally called u), 16 octahedral sites (M), and 8 tetrahedral sites (T) occupied by B and A cations, respectively. Only the lattice parameter (a) and the oxygen coordinate (u) are required to determine the atomic positions of this structure, thus fully defining the resulting tetrahedral (T-O) and octahedral (M-O) bond lengths. Atoms at tetrahedral and octahedral sites occupy special positions defined by the setting choice for the origin in the $Fd\bar{3}m$ space group, i.e., point symmetries $\bar{4}3m$ for a tetrahedral site or $\bar{3}m$ for an octahedral position (Sickafus et al. 1999).

The A and B site cation occupancy can be expressed as follows:

$$^{T}(A_{1-x}B_x)\ ^{M}[A_xB_{2-x}]\ O_4$$

where x is taken as the inversion parameter typifying the spinel structure in terms of normal or inverse. From the previous formula, the spinel structure can assume two extreme configurations; the normal spinel ($x = 0$) implies that the A and B cations are fully separated in T and M sites, respectively, whereas in the so-called inverse spinel ($x = 1$) all of the A and half of the B cations are placed in octahedral M site with the remaining B cations occupying the tetrahedral T site. When the degree of inversion is $x = 2/3$ the cations assume a completely random distribution between ^{IV}T- and ^{VI}M-sites. A spinel with an inversion parameter comprised between 0 and 2/3 is "largely normal," whereas another one with an inversion parameter $2/3 < x < 1$ is "largely inverse" (Nakatsuka et al. 2003). The inversion parameter is primarily affected by the temperature at which a given spinel is equilibrated and by its chemical composition (e.g., O'Neill 1994; O'Neill and Dollase 1994; Nakatsuka et al. 2003). When considering solid solutions among two spinel end-members having different values of the inversion degree, the variation along the join of this parameter complicates the study of structural relaxation due to the concurrent effects of cation substitution in one site and cation ordering over two sites. This explains why, in spite of the complete solid solutions well known in many different spinel systems, the investigation of structural relaxation is limited to the relatively few cases mentioned above.

In the present study, the combined X-ray diffraction (XRD) and electronic absorption spectroscopy (EAS) approach is applied to explore the effects of the Co for Zn substitution along the gahnite ($ZnAl_2O_4$)-Co-aluminate ($CoAl_2O_4$) solid-solution series. This is a first step to understand in depth the relaxation around the Co^{2+} ion of different structures with tetrahedral sites and to which extent this phenomenon affects the resulting coloration that finds important application once synthetic analogs are used as pigments.

Experimental methods

Samples synthesis

Five polycrystalline samples were prepared through solid-state reaction synthesis according to the formula $(Zn_{1-y}Co_y)Al_2O_4$, where $y = 0.00$, 0.25, 0.50, 0.75, and 1.00 apfu. High-purity binary oxides (ZnO, Co_3O_4, and Al_2O_3), used as raw materials, were mixed in ethanol in stoichiometric proportion, dried in an oven at 105 °C, pulverized in an agate mortar, pelletized, then calcined in sealed alumina crucible in an electric kiln in static air at maximum temperature of 1300 °C for eight hours after applying a heating rate of 3 °C/min. Although largely normal spinels, both gahnite and Co-aluminate end-members, as well as the samples of intermediate composition, exhibit a variable degree of cation exchange between tetrahedral and octahedral sites. It was demonstrated that the spinel inversion parameter increases when the specimen quenching temperature grows (e.g. O'Neill 1994; O'Neill and Dollase 1994; Nakatsuka et al. 2003). Therefore, to obtain the most accurate degree of relaxation around substituting cobalt in the tetrahedral site and therefore minimize the inversion parameter, all samples were slowly cooled to room temperature (Hirota et al. 1990; Tristan et al. 2005).

XRD data collection and structural refinements

Experimental data were collected at room temperature in the 5–130 °2θ angular range, with 0.015 °2θ scan rate, and 10 s per step counting time, on a Bruker D8 Advanced diffractometer equipped with a Si(Li) solid-state detector set to discriminate Cu$K\alpha_{1,2}$ radiation.

Rietveld structural refinements were performed using the GSAS-EXPGUI software package (Larson and Von Dreele 1988; Toby 2001) in the space group $Fd\bar{3}m$ with origin set at $\bar{3}m$, starting from the model (i.e., unit-cell parameter, a; oxygen atomic coordinate, u) taken from O'Neill and Dollase (1994). The diffraction peak profiles were modeled by a pseudo-Voigt function with the peak cut-off set to 0.05% of the peak maximum. The refined profile parameter included the θ-independent Gaussian (GW), and the two $(\cos\theta)^{-1}$- and (tanθ)-dependent Lorentzian (i.e., LX, and LY, respectively) broadening coefficients plus an asymmetry contribution. Besides the 18 shifted Chebyshev polynomial coefficients to reproduce the background, the refinements included a scale factor, the cell parameter (a), T and M site occupancies (i.e., the inversion parameter, x), the oxygen coordinate (u), and isotropic atomic displacement parameters (U_{iso}). Due to the high mutual correlations, the latter three variables were varied in alternate cycles. Cations hosted in the same coordination site (tetrahedron or octahedron) were constrained to maintain the chemical composition and to change the isotropic temperature factors identically. Finally, to improve both reliability indices and electron density distribution, the refinements were performed by using the ionized scattering factors of Zn^{2+}, Co^{2+}, Al^{3+}, and O^{2-} instead of that for neutral atoms (Ballirano 2003; Nakatsuka et al. 2003). Agreement factors, refinement details, and structural parameters are summarized in Table 1.

Electronic absorption spectroscopy

Optical measurements were performed by diffuse reflectance (Perkin Elmer λ19 spectrophotometer, 300–2500 nm range, 0.1 nm step size, $BaSO_4$ integrating sphere, white reference material: $BaSO_4$ pellet). Reflectance (R_∞) was converted to absorbance (K/S) by the Kubelka-Munk equation: $K/S = (1 - R_\infty)^2 \cdot (2R_\infty)^{-1}$ (Marfunin 1979). Absorbance bands were deconvoluted by a Gaussian function (PFM, OriginLab) starting from peak maxima by automatic fitting to convergence, to obtain band energy (centroid), which experimental error, including background correction and reproducibility, is around 1%. High-energy tails of bands, here interpreted as vibronic effects, may partly be spurious signal due to sample preparation. Crystal field strength $10Dq$ was calculated for Co^{2+} ions (d^7) by fitting the energy of spin-allowed transitions in the d^3 Tanabe-Sugano diagram which is used, according to the d^{10-x} rule, in the case of ions in fourfold coordination (Tanabe and Sugano 1954; Andrut et al. 2004). The effect of spin-orbit coupling was accounted by both averaging values of split bands and the baricenter method (Burns 1993); the results given by the two methods differ by less than 0.5%. The interelectronic repulsion Racah B parameter was evaluated by spin-allowed transitions (Lever 1984; Wildner et al. 2004) and the correspondent nephelauxetic ratio β (considered to express the covalent degree of the T-O bonding) was calculated as $\beta = B/B_0$, where B is experimental and B_0 is the free ion value (Lever 1984; Burns 1993).

Results and discussion

Crystal structure

In our synthesis conditions, five compounds of Co-doped gahnite with spinel structure were obtained; no impurities were detected. The structural incorporation of cobalt in the gahnite lattice is evidenced by the progressive and linear increase of the unit-cell parameter (a) as a function of the increasing nominal cobalt content (Fig. 1a). A similar trend has been previously

TABLE 1. $ZnAl_2O_4$-$CoAl_2O_4$ (space group $Fd\bar{3}m$; Z = 8): Goodness of fit (agreement factors), refinement details, and structural parameters with their standard deviations (in parentheses)

Nominal cobalt content, *y* (apfu):					
	0.00	0.25	0.50	0.75	1.00
Agreement factors and refinement details:					
χ^2	1.714	1.467	1.253	1.035	1.149
R_{wp}	0.1352	0.0951	0.0868	0.1023	0.0682
R_p	0.0843	0.0673	0.0660	0.0791	0.0532
No. of data	8333	8333	8333	8333	8333
No. of variables	28	35	35	35	34
R(*F*)	0.0268	0.0292	0.0304	0.0549	0.0412
R(F^2)	0.0300	0.0326	0.0354	0.0641	0.0414
No. of reflections	68	68	68	68	68
Structural parameters:					
a (Å)	8.08514(10)	8.09014(10)	8.09491(7)	8.10011(13)	8.10559(8)
u (adim.)	0.26446(9)	0.26430(9)	0.26415(12)	0.26397(20)	0.26384(19)
x	0.000	0.025	0.036	0.049	0.072
Isotropic displacement parameter, U_{iso} (Å^2):					
T	0.0053(2)	0.0050(2)	0.0052(3)	0.0048(4)	0.0050(4)
M	0.0028(3)	0.0044(4)	0.0045(4)	0.0058(6)	0.0063(5)
O	0.0065(5)	0.0062(9)	0.0053(6)	0.0080(9)	0.0079(8)

Notes: *a* = unit-cell parameter; *u* = oxygen coordinate; *x* = inversion parameter.

reported by other authors (Tristan et al. 2005; Gaudon et al. 2009; Popović et al. 2009; Duan et al. 2011), in one case with a non-linear relationship (see the data from Popović et al. 2009 reported on Fig. 1a for comparison).

As pointed out by Popović et al. (2009), this unit cell increasing trend cannot be explained on the base of the ionic radii difference if just the tetrahedral exchange between zinc and cobalt is considered. In fact, as the Shannon (1976) ionic radius for tetrahedrally coordinated Zn^{2+} (0.60 Å) is bigger than that of Co^{2+} (0.58 Å), an opposite trend would be expected. Therefore, Popović et al. (2009) suggested that cobalt incorporation in the gahnite structure has to be accompanied by an intersite-cation exchange, as quantified by the increasing inversion parameter (Fig. 1b), and concluded that the main cause of lattice expansion should be attributed to the Co^{2+} for Al^{3+} substitution in the octahedral site (i.e., the radius of sixfold-coordinated Al^{3+}, 0.535 Å, is much smaller than that of high-spin Co^{2+}, 0.745 Å).

On the other hand, the zinc-oxygen bond distance needs to be taken into consideration. Bosi et al. (2011) recently showed that in ZnM_2O_4 normal spinels (with M = Al, Cr, Ga, V, and Fe) the covalence degree of $^{[IV]}$Zn-O distances decreases with increasing size of the cation hosted in the octahedral site (MO_6) due to the smaller charge density of the M ion. As a matter of fact, while the reported $^{[IV]}$Zn-O bond length for the $ZnFe_2O_4$ perfectly matches the value obtained through the sum of the Shannon ionic radii (i.e., $\langle Zn\text{-}O\rangle_{observed}$ = 1.980 Å; and $Zn\text{-}O_{Shannon} = {}^{[IV]}Zn^{2+} + {}^{[IV]}O^{2-}$ = 0.60 + 1.38 = 1.98 Å), the tetrahedral bond distance of the other selected compounds becomes shorter as a function of the octahedral ion size, to the minimum value of $\langle Zn\text{-}O\rangle$ = 1.9493(6) Å for the $ZnAl_2O_4$ (Bosi et al. 2011). Considering this latter value as equal to 1.95 Å, it follows that the radius of the zinc ion in such an environment can be taken as shortened by 0.03 Å (therefore equal to 0.57 Å) due to the increased covalence degree of the Zn-O bond. The enhanced covalency of the Zn-O bond for zinc in tetrahedral coordination was earlier invoked in hardystonite by Louisnathan (1969) who suggested that the strong hybridization of sp^3 orbitals promotes particularly short Zn-O distances. Other evidences of the enhanced covalence character of the fourfold coordinated zinc were recently observed and described in silicate systems, such as Co-doped willemite, $^{[IV]}(Zn,Co)_2SiO_4$ (Ozel et al.

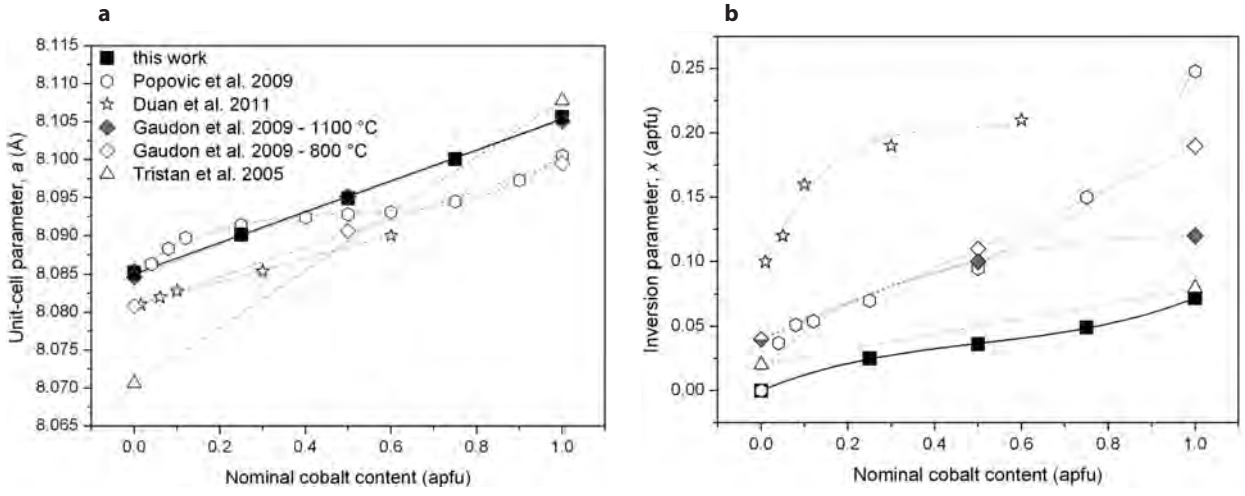

FIGURE 1. The *a* unit-cell edge (**a**) and the *x* inversion parameter (**b**) of Co-doped gahnite spinels as a function of the nominal cobalt content. Standard deviation is within the symbol size.

2010) and hardystonite, $Ca_2^{[IV]}(Zn,Co)Si_2O_7$ (Dondi et al. 2011), where an unexpected expansion of the unit-cell parameters were observed and ascribed to a reduction of the covalence effect induced by the Co for Zn substitution.

In Figure 1b, the variation of the inversion parameter, *x*, is illustrated as a function of the cobalt amount, for the same $ZnAl_2O_4$-$CoAl_2O_4$ joins previously described and reported in Figure 1a. Despite the heterogeneity of the plotted data due to the different conditions adopted to obtain the synthesized samples, the inversion parameter shows a gradual increase as a function of the cobalt content. Through the solid-state reaction synthesis (i.e., the join subject of this study as well as the samples synthesized by Tristan et al. 2005) the inversion parameter values are the lowest when compared with those of the other joins. O'Neill (1994) and Nakatsuka et al. (2003) demonstrated that the inversion parameter in $CoAl_2O_4$ spinel increases as the specimen quenching temperature gets higher. On the basis of these studies it is possible to estimate that the spinel samples investigated in the present work reached the equilibrium condition at about 700 °C.

At a first approximation, the Co ↔ Al intersite exchange provides a satisfactory explanation to describe the mean metal-oxygen bond length variations for both TO_4 and MO_6 polyhedra. The variation of the polyhedral bond length is linearly correlated with the increase of the unit-cell parameter (*a*). Data shown in Figure 2 indicate that the tetrahedral site undergoes a small but regular shortening of the bond distances, whereas the octahedron expands linearly, thus behaving in the opposite way. These trends can be well described by the simultaneous cationic substitution occurring in both polyhedral sites (i.e., while Co^{2+} and Al^{3+}, both smaller than zinc ion, substitute Zn^{2+} in T, the bigger Co^{2+} replaces the smaller Al^{3+} in M, through the relation:

$$^{T}(Zn_{1-y}Co_{y-x}Al_x)\ ^{M}[Co_xAl_{2-x}]\ O_4 \quad (2)$$

where *y* is the nominal cobalt content and *x* is the inversion parameter.

In Table 2, the mean polyhedral bond lengths obtained through the Rietveld refinements are compared to those calculated using the Shannon ionic radii for all ions except Zn for which, as previously discussed, a corrected radius equal to 0.57 Å was used. The comparison of the observed and the calculated values reveals that both tetrahedral ⟨T-O⟩ and octahedral ⟨M-O⟩ observed bond distances are satisfactorily approximated by the calculated bond lengths from ionic radii sums. It must be noted that the refined ⟨Zn-O⟩ bond distance in our study, 1.953 Å, statistically agrees with the value of 1.949 Å obtained by Bosi et al. (2011) using single-crystal diffraction. It is noteworthy that also the polyhedral bond length trends observed along the $ZnAl_2O_4$-$CoAl_2O_4$ solid solution in the work of Popović et al. (2009) can be described in a similar way, regardless of the cation inversion degree between tetrahedral and octahedral sites (see Table A[1] in appendix).

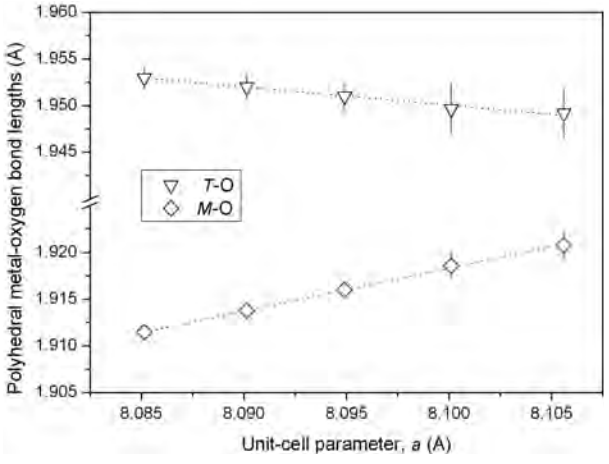

FIGURE 2. Polyhedral metal-oxygen bond lengths along the $ZnAl_2O_4$-$CoAl_2O_4$ solid solution as a function of the unit-cell parameter.

Electronic absorption spectroscopy

The optical spectra of Co-doped gahnites exhibit several absorption bands (Fig. 3) whose interpretation is not straightforward, because they originate from different phenomena (Ferguson et al. 1969; Marfunin 1979):

(1) Purely electronic transitions of Co^{2+} in tetrahedral coordination involve three spin-allowed bands: $^4T_2(^4F) \leftarrow {}^4A_2$, $^4T_1(^4F) \leftarrow$, and $^4T_1(^4P) \leftarrow$, plus several spin-forbidden bands (Lever 1984; Burns 1993; Brunold et al. 1996; Taran et al. 2009).

[1] Deposit item AM-12-053, Deposit Table and CIFs. Deposit items are available two ways: For a paper copy contact the Business Office of the Mineralogical Society of America (see inside front cover of recent issue) for price information. For an electronic copy visit the MSA web site at http://www.minsocam.org, go to the *American Mineralogist* Contents, find the table of contents for the specific volume/issue wanted, and then click on the deposit link there.

TABLE 2. $ZnAl_2O_4$-$CoAl_2O_4$: Comparison between observed and calculated (from ionic radii of Shannon 1976) polyhedral bond lengths in gahnite-Co-aluminate solid solution as a function of the inversion parameter (*x*)

Nominal cobalt content, *y* (apfu)	*x*	⟨T-O⟩$_{Obs}$ (Å)	⟨T-O⟩$_{Calc}$ (Å)	T$_{(Obs-Calc)}$ (Å)	⟨M-O⟩$_{Obs}$ (Å)	⟨M-O⟩$_{Calc}$ (Å)	M$_{(Obs-Calc)}$ (Å)
0.00	0.000	1.9530(12)	1.950	0.003	1.9115 (6)	1.915	-0.004
0.25	0.025	1.9520(13)	1.948	0.004	1.9138 (7)	1.918	-0.004
0.50	0.036	1.9510(16)	1.948	0.003	1.9160 (8)	1.919	-0.003
0.75	0.049	1.9497(28)	1.948	0.002	1.9186(14)	1.920	-0.002
1.00	0.072	1.9492(27)	1.946	0.003	1.9208(14)	1.923	-0.002
δ (Å)		*0.004*	*0.004*		*0.009*	*0.008*	

Notes: *x*: inversion parameter; ⟨T-O⟩$_{Obs}$ and ⟨M-O⟩$_{Obs}$: mean tetrahedral and octahedral bond lengths from Rietveld refinements with standard deviations (in parentheses); ⟨T-O⟩$_{Calc}$ and ⟨M-O⟩$_{Calc}$: mean tetrahedral and octahedral bond lengths, calculated from Shannon ionic radii as
⟨T-O⟩$_{Calc}$ = [(1 – *y*)·(i.r.$^{IV}Zn^{2+}$)] + [(*y* – *x*)·(i.r.$^{IV}Co^{2+}$)] + [(*x*)·(i.r.$^{IV}Al^{3+}$)] + (i.r.$^{IV}O^{2-}$),
where i.r.$^{IV}Zn^{2+}$ = 0.57 Å (see text for explanation) and
⟨M-O⟩$_{Calc}$ = [(*x*/2)·(i.r.$^{VI}Co^{2+}$)] + {[1 – (*x*/2)]·(i.r.$^{VI}Al^{3+}$)} + (i.r.$^{IV}O^{2-}$);
T$_{(Obs-Calc)}$, M$_{(Obs-Calc)}$: difference between observed and calculated bond distances for ⟨T-O⟩ and ⟨M-O⟩, respectively; and in italic, δ = maximum polyhedral deviation (i.e., the difference between the maximum and the minimum bond lengths).

(2) The contribution of cobalt ions in octahedral coordination, as expected from the inversion parameter in the Co-doped samples, is completely hidden by the overwhelming bands of fourfold-coordinated Co^{2+}. In fact, the Co^{2+} main optical transitions are predictable to occur at the spinel octahedron around 8000 cm^{-1} for $^4A_{2g}(^4F)$ and around 19 000 cm^{-1} for $^4T_{1g}(^4P)$ according to literature data (Burns 1993); these two bands would fall under the complex structures at 6000–10 000 and 16 000–20 000 cm^{-1}, respectively (Fig. 3).

(3) A strong spin-orbit coupling, expected for d^7 ions, leads to a conspicuous splitting of the Co^{2+} bands: the spin-allowed ones are found threefold split and even a limited mixing of $^4T_2$ and $^4T_1$ states is claimed (Ferguson et al. 1969).

(4) The occurrence of spin-forbidden transitions with an energy close to that of the spin-allowed $^4T_1(^4P)$ one causes a mixing of quadruplet and doublet states (Ferguson et al. 1969; Sardar et al. 2002). This circumstance leads to a consistent intensity gain of spin-forbidden bands, which overlap those from the split spin-allowed transitions, making any accurate estimation of their energy very hard.

(5) Vibronic effects are systematically registered as sidebands generated by band splitting and mixing of states. These effects, although individually discernible in low-temperature spectra (Ferguson et al. 1969; Brunold et al. 1996), induce at room temperature an apparent broadening of electronic transition bands.

A more detailed spectral interpretation allows the distinction of four regions (Fig. 3).

(I) In the 4000–6000 cm^{-1} range, the $^4T_2(^4F)$ transition gives rise to two split bands (one measurable at 4150 cm^{-1} and another very broad around 4000 cm^{-1}) overlapped by vibronic effects. The main component of the threefold split $^4T_2$ is expected to fall just below the detection window of our equipment, i.e., ~3990 cm^{-1} (Ferguson et al. 1969; Deren et al. 1994; Sardar et al. 2002).

(II) In the 6000–9000 cm^{-1} interval there is a complex structure where the $^4T_1(^4F)$ transition is split into three components (around 6700, 7200, and 7600 cm^{-1}, respectively), which are associated to various vibronic sidebands (Fig. 4a).

(III) The 15 000–20 000 cm^{-1} region is particularly complicated (Fig. 4b): here the quadruplet $^4T_1(^4P)$ transition overlaps four doublet transitions originated from the ^2G term: ^2E, $^2T_1$, $^2T_2$, and $^2A_1$. The $^4T_1$ transition is threefold split into the 16 000–17 000 cm^{-1} range, where only two bands are clearly distinguished, although the first one is strongly mixed with the ^2E and $^2T_1$ states. A third band at about 18 500 cm^{-1} is attributed to both the $^2A_1$ and $^2T_2$ spin-allowed transitions, whose anomalous intensity stems from vibronic effects in the 17 000–18 000 cm^{-1} interval.

(IV) Spin-forbidden transitions occur in the high-energy part of spectra (over 20 000 cm^{-1}): only two weak bands are discernible and attributed to $^2T_1(^2P)$ at ~21 000 cm^{-1} and $^2T_1(^2H)$ at ~24 500 cm^{-1}.

The energies of individual transitions are comparable with those of Co-bearing spinels from the literature (Table 3).

Crystal field strength is slightly decreasing with increasing cobalt amount: 10*Dq* goes from 4187 to 4131 cm^{-1} (Table 3). These results fit the 10*Dq* range of the literature for synthetic analogs, i.e., 4100–4230 cm^{-1} for Co-doped $ZnAl_2O_4$ (Ferguson et al. 1969; Duan et al. 2003); 4000–4200 cm^{-1} for Co-doped $MgAl_2O_4$ (Burns 1993; Kuleshov et al. 1993; Duan et al. 2004; Taran et al. 2009; Nataf et al. 2009) and 4280 cm^{-1} for $CoAl_2O_4$ (Torres et al. 2007). Overall, crystal field data appear to be rather variable, even once referred to the same spinel with a comparable amount of cobalt, as a consequence of uncertainty in the energy evaluation of split bands in such complicated optical spectra.

The Racah *B* parameter fluctuates in the 744–751 cm^{-1} range (Table 3) corresponding to a nephelauxetic ratio around $\beta = 0.77$, which implies that a significant degree of covalency affects the Co-O bond, but also that no appreciable change of such a covalency occurs along the join. These values match the known interval for synthetic spinel *ss* and gahnite that ranges from 730 to 790 cm^{-1} (Ferguson et al. 1969; Kuleshov et al. 1993; Duan et al. 2003, 2004; Torres et al. 2007; Nataf et al. 2009).

In the samples under investigation, the spin-forbidden $^2E(^2G)$ transition is superimposed by the spin-allowed $^4T_2(^4P)$ so it is impossible to get a direct assessment of the Racah *C* parameter. It is estimated to be around 3375 cm^{-1} on the basis of the $C = 4.5B$ relationship (Lever 1984).

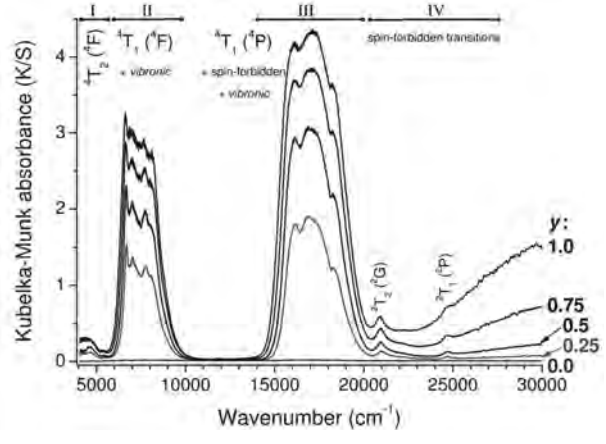

FIGURE 3. Optical spectra of the $ZnAl_2O_4$-$CoAl_2O_4$ solid solution (*y*: nominal cobalt content, apfu). Main electronic transitions are indicated together with regions I–IV described in the text.

Structural relaxation

The most popular method to achieve the local metal-oxygen distances in a solid solution investigated through electronic absorption spectroscopy is by means of the crystal field parameter 10*Dq* (e.g., Langer 2001; Langer et al. 2004; Taran et al. 2004; Cruciani et al. 2009; Hålenius et al. 2010, 2011). The 10*Dq* of 3*d*-ions depends on the mean metal-oxygen bond distances by

$$10Dq = \text{const}\cdot(\langle \text{T-O} \rangle)^{-5} \quad (3)$$

where the constant comprises both the effective charge on the ligand, Q, and the average radius of the *d* orbital, ⟨r⟩, which are constant for a given metal ion in a given ligand environment (Dunn et al. 1965; Marfunin 1979; Burns 1993).

It is worth to point out that, while the local tetrahedral bond length variation observed through optical spectroscopy is exclusively a function of the cobalt for zinc substitution in the T site, the average tetrahedral bond distances obtained by X-ray diffraction are affected by the cationic Co-Al intersite exchange

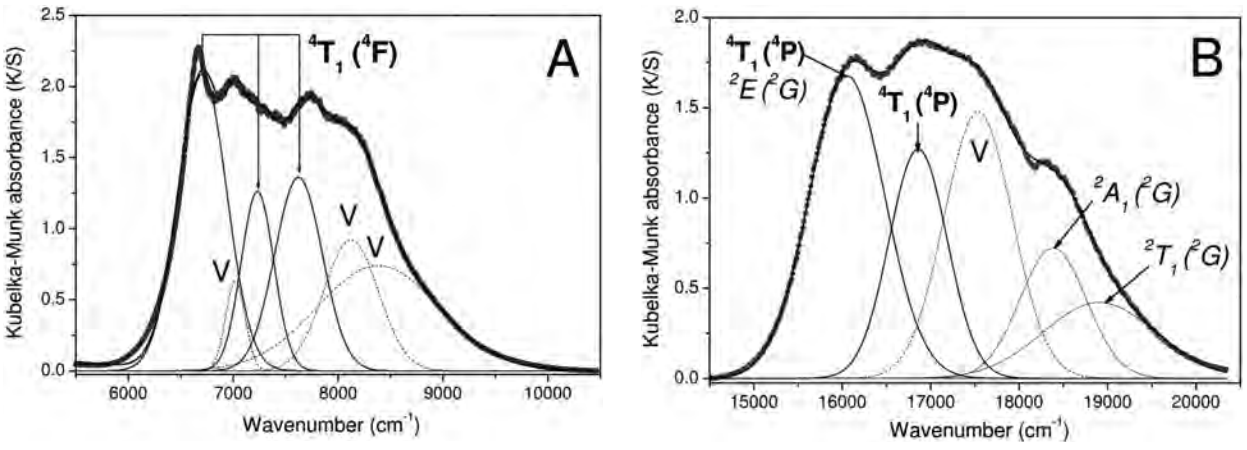

FIGURE 4. Optical spectra interpreted by deconvolution of individual bands in the 6000–10 000 (**a**) and 15 000–20 000 cm^{-1} ranges (**b**). Electronic transitions are indicated (V = vibronic transitions). Examples refer to sample $Zn_{0.75}Co_{0.25}Al_2O_4$.

TABLE 3. Optical properties of the gahnite-Co-aluminate solid solution compared with literature data on aluminate spinels

	This work				A	B	C	D	E
Nominal cobalt content, *y* (apfu)	0.25	0.50	0.75	1.00	~0.03	~0.01	0.03	~1.0	~0.1
Cobalt in tetrahedral coordination (apfu)	0.23	0.46	0.70	0.93	$ZnAl_2O_4$	$MgAl_2O_4$	$MgAl_2O_4$	$CoAl_2O_4$	$MgAl_2O_4$
Energy of transition bands (cm^{-1})									
$^4T_2$ (^4F)	n.d.	n.d.	n.d.	n.d.	**3967**	n.d.	**3970**	n.d.	n.d.
$^4T_2$ (^4F)	n.d.	n.d.	n.d.	n.d.	**4062**	n.d.	**4085**	n.d.	n.d.
$^4T_2$ (^4F)	**4179**	**4151**	**4134**	**4116**	**4255**	n.d.	**4441**	n.d.	**~4200**
Vibronic	*4660*	*4630*	*4610*	*4590*	*4320*	n.d.	*4623*	n.d.	n.d.
$^4T_1$ (^4F)	**6720**	**6710**	**6700**	**6670**	**6756**	**6400**	**6510**	**6555**	**6640**
Vibronic	*7070*	*7020*	*7020*	*7000*	*6990*	n.d.	n.d.	n.d.	n.d.
$^4T_1$ (^4F)	**7320**	**7230**	**7260**	**7220**	**7072**	**7200**	**7057**	n.d.	**7070**
$^4T_1$ (^4F)	7680	7620	7620	7580	7776	8000	7407	7518	7730
Vibronic	*8110*	*8120*	*8080*	*8140*	*8050*	n.d.	*8137*	*8240*	n.d.
Vibronic	*8510*	*8380*	*8470*	*8350*	*8220*	n.d.	n.d.	n.d.	n.d.
^2E (^2G)	n.d.	n.d.	n.d.	n.d.	15732	n.d.	14900	n.d.	n.d.
$^4T_1$ (^4P) plus $^2T_1$ (^2G)	**16050**	**16010**	**15930**	**15760**	**16040**	**15900**	**16000**	**15625**	**16080**
$^4T_1$ (^4P)	**16860**	**16870**	**16860**	**16760**	**16210**	**16700**	**16722**	**16900**	**16840**
Vibronic	*17540*	*17530*	*17530*	*17510*	*16590*	*17200*	*17241*	n.d.	n.d.
$^2A_1$ (^2G) plus vibronic	18380	18340	18370	18350	18250	18300	18348	18300	18260
$^2T_2$ (^2G)	18910	18880	18490	18710	18670	n.d.	n.d.	n.d.	n.d.
$^2T_1$ (^2P)	21020	20980	20960	20900	21020	n.d.	21053	20500	20920
$^2T_1$ (^2H)	24720	24690	24680	24650	24741	n.d.	n.d.	n.d.	n.d.
Crystal field strength, 10Dq (cm^{-1})	**4187**	**4156**	**4150**	**4131**	**~4100**	**4000**		**4280**	**~4200**
Racah *B* parameter (cm^{-1})	**751**	**753**	**751**	**744**	**733**	**730**		**741**	**600**

Notes: n.d. = not determined. Measured values have an estimated uncertainty around 1%. Spin-allowed transitions are in bold, while vibronic bands are in italic.
References: A = Ferguson et al. (1969); B = Kuleshov et al. (1993); C = Sardar et al. (2002); D = Torres et al. (2007); E = Taran et al. (2009).

which is mainly responsible for their shortening as the Co for Zn replacement increases. Hence, to obtain the most reliable comparison between mean and local tetrahedral bond lengths around the Co ion, the effect due to the occurrence of a small fraction of tetrahedral sites filled by Al must be corrected for. To perform this correction, the calculated $\langle T\text{-}O\rangle_{calc}$ bond distances, reported in Table 2, were recast as to a completely normal cation distribution, eliminating the effects of the inversion degree (see the $\langle T\text{-}O\rangle_{x=0}$ bond length listed in Table 4). By using the so recast $\langle T\text{-}O\rangle_{x=0}$ bond lengths, the local Co-oxygen distances, $\langle Co\text{-}O\rangle^{Local}$, were easily determined from optical spectroscopy data by means of the Equation 3, through:

$$\langle Co\text{-}O\rangle^{Local} = \langle T\text{-}O\rangle_{y=1} \cdot [(10Dq Co^{2+})_{y=1}/(10Dq Co^{2+})_y]^{1/5}. \quad (4)$$

The relaxation coefficient (ε) for the $ZnAl_2O_4$-$CoAl_2O_4$ solid solution was therefore quantified by plotting both the $\langle Co\text{-}O\rangle^{Local}$ and the $\langle T\text{-}O\rangle_{x=0}$ vs. the nominal cobalt content (i.e., Fig. 5) and calculated as

$$\varepsilon = (\langle Co\text{-}O\rangle^{Local} - \langle T\text{-}O\rangle_{y=0}) \cdot (\langle T\text{-}O\rangle_{y=1} - \langle T\text{-}O\rangle_{y=0})^{-1} = 0.47. \quad (5)$$

With the minimal tetrahedral bond length of 1.9535 Å, extrapolated for an infinite dilution of cobalt in the solid solution (i.e., $\varepsilon_{lim(y)} \rightarrow 0$) and maximal $\langle Co\text{-}O\rangle^{Local}$ distance of 1.960 Å, the relaxation coefficient obtained in the present study is ε = 0.47. To evaluate the effects of assuming different sets of ideal distances on modeling the variation of mean tetrahedral bond lengths between the two end-members, another calculation of the structural relaxation coefficient was performed using the ideal tetrahedral bond distances reported by Lavina et al. (2002) for gahnite (^{IV}Zn-O = 1.960) and Co-aluminate (^{IV}Co-O = 1.972). A value of ε = 0.56 resulted from this calculation. The variation of the structural relaxation along the $Zn_{1-y}Co_yAl_2O_4$ spinel solid

TABLE 4. $ZnAl_2O_4$-$CoAl_2O_4$: Observed and calculated tetrahedral bond lengths in gahnite-Co-aluminate solid solution

Nominal cobalt content, *y* (apfu)	$\langle T\text{-}O\rangle_{Obs}$ (Å)	$\langle T\text{-}O\rangle_{Calc}$ (Å)	$\langle T\text{-}O\rangle_{x=0}$ (Å)	$\langle Co\text{-}O\rangle^{Local}$ (Å)
0.00	1.9530(12)	1.950	1.950(1)	-
0.25	1.9520(13)	1.948	1.953(2)	1.955(2)
0.50	1.9510(16)	1.948	1.955(2)	1.958(2)
0.75	1.9497(28)	1.948	1.958(2)	1.958(2)
1.00	1.9492(27)	1.946	1.960(3)	1.960(2)

Notes: $\langle T\text{-}O\rangle_{Obs}$: mean tetrahedral bond lengths from Rietveld refinements with standard deviations (in parentheses); $\langle T\text{-}O\rangle_{Calc}$: mean tetrahedral bond lengths, calculated as described in Table 2; $\langle T\text{-}O\rangle_{x=0}$: tetrahedral distances recast by considering the inversion parameter $x = 0$ over the whole solid solution; $\langle Co\text{-}O\rangle^{Local}$: tetrahedral Co-O bond distances calculated on the base of Equation 4 (see text for further details).

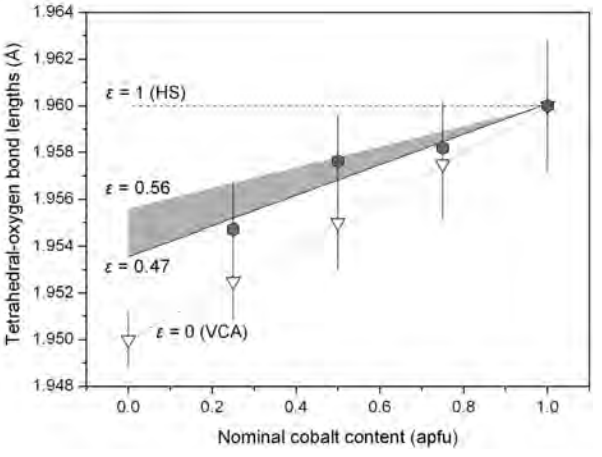

FIGURE 5. Coefficient of structural relaxation around $^{[IV]}Co^{2+}$ in the gahnite-Co-aluminate spinel solid solution. Empty triangles refer to the mean tetrahedral bond lengths $\langle T\text{-}O\rangle_{x=0}$ recast as for a completely normal cation distribution (see text for further details), whereas dark-gray filled hexagons are the local bond distances obtained through the electronic absorption spectroscopy. Gray filled area indicates the range of variation of the structural relaxation coefficient obtained by using data refined in this study ($\varepsilon = 0.47$) and the ideal values reported by Lavina et al. 2002 ($\varepsilon = 0.56$).

solution for the coefficient range of $0.47 \le \varepsilon \le 0.56$ is depicted by the shaded area in Figure 5. Notwithstanding the above uncertainties in establishing the accurate relaxation coefficient in spinel structure, the value we obtained for the gahnite-Co-aluminate join appears appreciably smaller than that calculated by Hålenius et al. (2011) for the fourfold-coordinated Mn^{2+} along the spinel *ss*-galaxite solid solution ($\varepsilon = 0.83$). A possible explanation for this difference might involve the above-mentioned enhanced degree of covalency for bonds involving the $^{IV}Zn^{2+}$ ion. Although the variation of $\langle T\text{-}O\rangle$ were corrected for the effect of increasing inversion parameter with Co content along the solid solution, a coupling of the two effects (i.e., covalency, and inversion) cannot be ruled out. In fact, the spinel *ss*-galaxite solid solution is characterized by an inversion parameter of ~0.24 on average along the entire investigated join, in a process that involves both the $Mg^{2+} \leftrightarrow Al^{3+}$ and, in a lesser degree, the $Mn^{2+} \leftrightarrow Al^{3+}$ intersite exchange (Hålenius et al. 2011). The join studied here seems to be more constrained by the strong preference of the Zn^{2+} for the tetrahedral site in which the metal can exert its enhanced covalency, thus limiting the cation exchange between tetrahedral and octahedral sites (i.e., x ~0.04 on the average) and the lattice flexibility. An analogous situation, which is useful to better understand how the Zn cation can be associated to a structural constraint in spinel structures, is that of the $MgAl_2O_4$-$MgCr_2O_4$ and $ZnAl_2O_4$-$ZnCr_2O_4$ solid solutions (Hålenius et al. 2010). Although characterized by the absence of a cationic inversion between tetrahedral and octahedral sites, and by having the same octahedral environment where Al^{3+} is progressively replaced by the bigger Cr^{3+}, the structural relaxation coefficient calculated for the gahnite-Zn-chromite join ($\varepsilon = 0.60$) is smaller than that obtained for the spinel *ss*-Mg-chromite solid solution ($\varepsilon = 0.69$).

ACKNOWLEDGMENTS

This study was carried out within a project founded by the "SPIN-GEO-TECH" PRIN program of the Italian Ministry for University and Research (MIUR). Authors are grateful to the Department of Industrial Chemistry and Materials, University of Bologna, for the access to its spectrophotometer laboratory.

REFERENCES CITED

Andrut, M., Wildner, M., and Rudowicz, C. (2004) Optical absorption spectroscopy in geosciences. Part II: Quantitative aspects of crystal fields. In A. Beran and E. Libowitzky, Eds., Spectroscopic Methods in Mineralogy, 6, p. 145–188. EMU Notes in Mineralogy, Eötvös University Press, Budapest.

Ballirano, P. (2003) Effects of the choice of different ionization level for scattering curves and correction for small preferred orientation in Rietveld refinement: the $MgAl_2O_4$ test case. Journal of Applied Crystallography, 36, 1056–1061.

Bosi, F., Andreozzi, G.B., Hålenius, U., and Skogby, H. (2011) Zn-O tetrahedral bond length variations in normal spinel oxides. American Mineralogist, 96, 594–598.

Brunold, T.C., Gudel, H.U., and Cavalli, E. (1996) Absorption and luminescence spectroscopy of Zn_2SiO_4 willemite crystals doped with Co^{2+}. Chemical Physics Letters, 252, 112–120.

Burns, R.G. (1993) Mineralogical Applications of Crystal Field Theory, 2nd ed., p. 576. Cambridge University Press, U.K.

Cruciani, G., Ardit, M., Dondi, M., Matteucci, F., Blosi, M., Dalconi, M.C., and Albonetti, S. (2009) Structural relaxation around Cr^{3+} in $YAlO_3$-$YCrO_3$ perovskites from electron absorption spectra. Journal of Physical Chemistry A, 113, 13772–13778.

Deren, P.J., Strek, W., Oetliker, U., and Güdel, H.U. (1994) Spectroscopic properties of Co^{2+} ions in $MgAl_2O_4$ spinels. Physica status solidi (b), 182, 241–251.

Dondi, M., Zanelli, C., Ardit, M., and Cruciani, G. (2011) Co-doped hardystonite, $Ca_2(Zn,Co)Si_2O_7$, a new blue ceramic pigment. Journal of the American Ceramic Society, 94, 1025–1030.

Duan, X.L., Yuan, D.R., Cheng, X.F., Sun, Z.H., Sun, H.Q., Xu, D., and Lv, M.K. (2003) Spectroscopic properties of Co^{2+}: $ZnAl_2O_4$ nanocrystals in sol-gel derived glass-ceramics. Journal of Physics and Chemistry of Solids, 64, 1021–1025.

Duan, X.L., Yuan, D.R., Cheng, X.F., Wang, Z.M., Sun, Z.H., Luan, C.N., Xu, D., and Lv, M.K. (2004) Absorption and photoluminescence characteristics of Co^{2+}:$MgAl_2O_4$ nanocrystals embedded in sol-gel derived SiO_2-based glass. Optical Materials, 25, 65–69.

Duan, X.L., Yuan, D.R., and Yu, F. (2011) Cation distribution in Co-doped $ZnAl_2O_4$ nanoparticles studied by X-ray photoelectron spectroscopy and ^{27}Al solid-state NMR spectroscopy. Inorganic Chemistry, 50, 5460–5467.

Dunn, T., McClure, D., and Pearson, R. (1965) Some Aspects of Crystal Field Theory, p. 115. Harper and Row, New York.

Ferguson, J., Wood, D.L., and Van Uitert, L.G. (1969) Crystal-field spectra of $d^{3,7}$ ions. V. Tetrahedral Co^{2+} in $ZnAl_2O_4$ spinel. Journal of Chemical Physics, 51, 2904–2910.

Galoisy, L. (1996) Local versus average structure around cations in minerals from spectroscopic and diffraction measurements. Physics and Chemistry of Minerals, 23, 217–225.

Gaudon, M., Apheceixborde, A., Ménétrier, M., Le Nestour, A., and Demourgues, A. (2009) Synthesis temperature effect on the structural features and optical absorption of $Zn_{1-x}Co_xAl_2O_4$ oxides. Inorganic Chemistry, 48, 9085–9091.

Gaudry, É., Sainctavit, P., Juillot, F., Bondioli, F., Ohresser, P., and Letard, I. (2006) From the green color of eskolaite to the red color of ruby: an X-ray absorption spectroscopy study. Physics and Chemistry of Minerals, 32, 710–720.

Hålenius, U., Andreozzi, G., and Skogby, H. (2010) Structural relaxation around Cr^{3+} and red-green color change in the spinel (sensu stricto)-magnesiochromite ($MgAl_2O_4$-$MgCr_2O_4$) and gahnite-zincochromite ($ZnAl_2O_4$-$ZnCr_2O_4$) solid-solution series. American Mineralogist, 95, 456–462.

Hålenius, U., Bosi, F., and Skogby, H. (2011) A first record of strong structural

relaxation of TO_4 tetrahedra in a spinel solid solution. American Mineralogist, 96, 617–622.
Hirota, K., Inoue, T., Mochida, N., and Ohtsuka, A. (1990) Study of germanium spinels (Part 3). Journal of the Ceramic Society of Japan, 98, 976–986.
Juhin, A., Calas, G., Cabaret, D., and Galoisy, L. (2007) Structural relaxation around substitutional Cr^{3+} in $MgAl_2O_4$. Physical Review B, 76, 054105.
Juhin, A., Calas, G., Cabaret, D., Galoisy, L., and Hazemann, J.-L. (2008) Structural relaxation around substitutional Cr^{3+} in pyrope garnet. American Mineralogist, 93, 800–805.
Kuleshov, N.Y., Mikhailov, V.P., Scherbitsky, V.G., Prokoshin, P.V., and Yumashev, K.V. (1993) Absorption and luminescence of tetrahedral Co^{2+} ion in $MgAl_2O_4$. Journal of Luminescence, 55, 265–269.
Langer, K. (2001) A note on mean distances, $R_{[MO6]}$, in substituted polyhedra, $[(M_{1-x}M_x')O_6]$, in the crystal structures of oxygen based solid solutions: local versus crystal averaging methods, Zeitschrift für Kristallographie, 216, 87–91.
Langer, K., Platonov, A., and Matsyuk, S. (2004) Local mean chromium-oxygen distances in Cr^{3+}-centered octahedra of natural grossular-uvarovite garnet solid solutions from electronic absorption spectra. Zeitschrift für Kristallographie, 219, 272–277.
Larson, A. and Von Dreele, R. (1988) General Structure Analysis System (GSAS). Los Alamos National Laboratory Report LAUR 86-748.
Lavina, B., Salviulo, G., and Della Giusta, A. (2002) Cation distribution and structure modelling of spinel solid solutions. Physics and Chemistry of Minerals, 29, 10–18.
Levelut, C., Ramos, A., and Petiau, J. (1991) EXAFS study of the local structure in CdS_xSe_{1-x} compounds. Materials Science and Engineering: B, 8, 251–263.
Lever, A.B.P. (1984) Inorganic Electronic Spectroscopy, 2nd ed., p. 863. Elsevier, Amsterdam.
Louisnathan, J. (1969) Refinement of the crystal structure of hardystonite, $Ca_2ZnSi_2O_7$. Zeitschrift für Kristallographie, 130, 427–437.
Marfunin, S. (1979) Physics of Minerals and Inorganic Materials, p. 340. Springer, Berlin.
Nakatsuka, A., Ikeda, Y., Yamasaki, Y., Nakayama, N., and Mizota, T. (2003) Cation distribution and bond lengths in $CoAl_2O_4$ spinel. Solid State Communications, 128, 85–90.
Nataf, L., Rodriguez, F., Valiente, R., and Ulanov, V. (2009) Optical characterization of fourfold (T_d)- and sixfold (O_h)-transition-metal species in $MgAl_2O_4$:Co^{2+} by time-resolved spectroscopy. Journal of Luminescence, 129, 1602–1605.
O'Neill, H.St.C. (1994) Temperature dependence of the cation distribution in $CoAl_2O_4$ spinel. European Journal of Mineralogy, 6, 603–609.
O'Neill, H.St.C. and Dollase, W. (1994) Crystal structures and cation distributions in simple spinels from powder XRD structural refinements: $MgCr_2O_4$, $ZnCr_2O_4$, Fe_3O_4 and the temperature dependence of the cation distribution in $ZnAl_2O_4$. Physics and Chemistry of Minerals, 20, 541–555.
Ozel, E., Yurdakul, M., Turan, S., Ardit, M., Cruciani, G., and Dondi, M. (2010) Co-doped willemite ceramic pigments: Technological behaviour, crystal structure and optical properties. Journal of the European Ceramic Society, 30, 3319–3329.
Popović, J., Tkalčec, E., Gržeta, B., Kurajica, S., and Rakvin, B. (2009) Inverse spinel structure of Co-doped gahnite. American Mineralogist, 94, 771–776.
Sardar, D.K., Gruber, J.B., Zandi, B., Ferry, M., and Kokta, M.R. (2002) Spectroscopic properties of Co^{2+} in related spinels. Journal of Applied Physics, 91, 4846–4852.
Shannon, R. (1976) Revised effective ionic radii and systematic studies of interatomic distances in halides and chalcogenides. Acta Crystallographica, A32, 751–767.
Sickafus, K., Wills, J., and Grimes, N. (1999) Structure of spinels. Journal of the American Ceramic Society, 82, 3279–3292.
Tanabe, Y. and Sugano, S. (1954) On the absorption spectra of complex ions. I and II. Journal of the Physical Society of Japan, 9, 753–779.
Taran, M., Langer, K., Abs-Wurmbach, I., Frost, D., and Platonov, A. (2004) Local relaxation around $^{[6]}Cr^{3+}$ in synthetic pyrope-knorringite garnets, $^{[8]}Mg_3{}^{[6]}(Al_{1-x}Cr_x{}^{3+})_2{}^{[4]}Si_3O_{12}$, from electronic absorption spectra. Physics and Chemistry of Minerals, 31, 650–657.
Taran, M.N., Koch-Müller, M., and Feenstra, A. (2009) Optical spectroscopic study of tetrahedrally coordinated Co^{2+} in natural spinel and staurolite at different temperatures and pressures. American Mineralogist, 94, 1647–1652.
Toby, H. (2001) EXPGUI, a graphical user interface for GSAS. Journal of Applied Crystallography, 34, 210–213.
Torres, F.J., Rodriguez-Mendoza, U.R., Lavin, V., de Sola, E.R., and Alarcon, J. (2007) Evolution of the structural and optical properties from cobalt cordierite glass to glass-ceramic based on spinel crystalline phase materials. Journal of Non-Crystalline Solids, 353, 4093–4101.
Tristan, N., Hemberger, J., Krimmel, A., Krug von Hidda, H.-A., Tsurkan, V., and Loidl, A. (2005) Geometric frustration in the cubic spinel MAl_2O_4 (M=Co, Fe, and Mn). Physical Review B, 72, 174404.
Urusov, V. (1992) A geometric model of deviations from Vegard's rule. Journal of Solid State Chemistry, 98, 223–236.
Wildner, M., Andrut, M., and Rudowicz, C. (2004) Optical absorption spectroscopy in geosciences. Part I: Basic concepts of crystal field theory. In A. Beran and E. Libowitzky, Eds., Spectroscopic Methods in Mineralogy, 6, p. 93–140. EMU Notes in Mineralogy, Eötvös University Press, Budapest.

Manuscript received January 5, 2012
Manuscript accepted April 8, 2012
Manuscript handled by Simon Redfern